Inorganic Chemistry
Article

Inorg. Chem. **2009**, *48*, 6055–6064 **6055**
DOI: 10.1021/ic9004328

Accessing the Different Redox States of α-Iminopyridines within Cobalt Complexes

Connie C. Lu,* Thomas Weyhermüller, Eckhard Bill, and Karl Wieghardt*

Max-Planck-Institut für Bioanorganische Chemie, Stiftstrasse 34-36, D-45470 Mülheim an der Ruhr, Germany

Received March 4, 2009

Cobalt coordination complexes featuring the redox-active α-iminopyridine ligand are described. The quite reducing bis(ligand)cobalt monoanion (**1**^{red}) was isolated and characterized by X-ray crystallography. The complex forms a three-membered electron-transfer series along with its neutral and monocationic counterparts, which were previously reported. The electronic structures in this series are all consistent with divalent cobalt and the redox events being ligand-centered. The reactivity profile of **1**^{red} was briefly explored, and two new compounds were isolated, bis(ligand)-methylcobalt (**2**) and bis(ligand)iodocobalt (**3**). Though **2** and **3** are isostructural, they are characterized by different electronic structures. The methylcobalt complex is best described by a Co(III) center with two ligand radicals, whereas the iodocobalt species is more aptly assigned as a Co(II) center with only one ligand radical. Further evidence of their different electronic structures is that a low-lying excited state is populated at room temperature in the case of the iodocobalt compound, whereas the methylcobalt complex is an energetically well-isolated spin singlet. Magnetic susceptibility data, structural data, variable temperature NMR spectroscopy, and density functional theory calculations lend support to this proposal.

I. Introduction

Bis(imino)pyridine is a versatile ligand for stabilizing reactive metal centers,[1] due in part to its capability to store electrons in its conjugated π/π^* system.[2,3] The truncated relative α-iminopyridine is also a common ligand, but it is primarily utilized as a neutral, diimine analogue (L^0). We and others have recently reported structural characterization of the monoanionic π^* radical form ($L^{\bullet-}$) of α-iminopyridine within coordination complexes.[4−6] The fully reduced state, which is the closed-shell dianion (L^{2-}), has also been structurally characterized albeit only in a few complexes of magnesium,[7] lanthanum, and neodymium.[8] Together, these three ligand types constitute the possible redox states of α-iminopyridines, and they can be readily distinguished based on the bond distances of the ligand backbone as illustrated in Scheme 1.

We presently focus on cobalt compounds containing two 2,6-diisopropylphenyl-substituted iminopyridine ligands. We demonstrate that this ligand is capable of spanning its full oxidation range from the neutral (L^0) to the dianionic state (L^{2-}) within one system. Also, we continue to investigate the issue of metal versus ligand oxidation by probing the electronic ramifications of altering a fifth ligand X in the coordination sphere of the cobalt center (where X = THF, Me^-, or I^-).

II. Experimental Section

All syntheses were carried out using standard glovebox and Schlenk techniques in the absence of water and dioxygen. Dry solvents were purchased from Fluka and degassed prior to use. THF-d_8 was purchased from Cambridge Isotope Laboratories, Inc., degassed via repeated freeze−pump−thaw cycles, and dried over activated 3 Å molecular sieves. Sodium metal was purchased from Aldrich and washed with hexanes prior to use. The reagents 15-crown-5, CH_3I, $^{13}CH_3I$, and $(n\text{-}Bu)_3SnI$ were purchased from commercial vendors and sparged with Argon prior to use. The ligand, 2,6-bis-(1-methylethyl)-*N*-(2-pyridinylmethylene)phenylamine[9] (abbreviated as L) was prepared according to the literature, as well as the neutral bis(ligand)cobalt complex $[(L^{\bullet-})_2Co]$ (**1**).[4]

*To whom correspondence should be addressed. E-mail: ccluck@mpi-muelheim.mpg.de (C.C.L.), wieghardt@mpi-muelheim.mpg.de (K.W.).

(1) Knijnenburg, Q.; Gambarotta, S.; Budzelaar, P. H. M. *Dalton Trans.* **2006**, 5442.
(2) Bart, S. C.; Chłopek, K.; Bill, E.; Bouwkamp, M. W.; Lobkovsky, E.; Neese, F.; Wieghardt, K.; Chirik, P. J. *J. Am. Chem. Soc.* **2006**, *128*, 13901.
(3) de Bruin, B.; Bill, E.; Bothe, E.; Weyhermüller, T.; Wieghardt, K. *Inorg. Chem.* **2000**, *39*, 2936.
(4) Lu, C. C.; Bill, E.; Weyhermüller, T.; Bothe, E.; Wieghardt, K. *J. Am. Chem. Soc.* **2008**, *130*, 3181.
(5) Trifonov, A. A.; Fedorova, E. A.; Borovkov, I. A.; Fukin, G. K.; Baranov, E. V.; Larionova, J.; Druzhkov, N. O. *Organometallics* **2007**, *26*, 2488.
(6) Lu, C. C.; DeBeer George, S.; Weyhermüller, T.; Bill, E.; Bothe, E.; Wieghardt, K. *Angew. Chem., Int. Ed.* **2008**, *47*, 6384.
(7) Westerhausen, M.; Bollwein, T.; Makropoulos, N.; Schneiderbauer, S.; Suter, M.; Nöth, H.; Mayer, P.; Piotrowski, H.; Polborn, K.; Pfitzner, A. *Eur. J. Inorg. Chem.* **2002**, 389.
(8) Sugiyama, H.; Korobkov, I.; Gambarotta, S.; Möller, A.; Budzelaar, P. H. M. *Inorg. Chem.* **2004**, *43*, 5771.
(9) Laine, T. V.; Klinga, M.; Leskelä, M. *Eur. J. Inorg. Chem.* **1999**, 959.

Published on Web 05/28/2009

Scheme 1. Different Redox States of the α-Iminopyridine Ligand with Their Characteristic Bond Distances (Å)

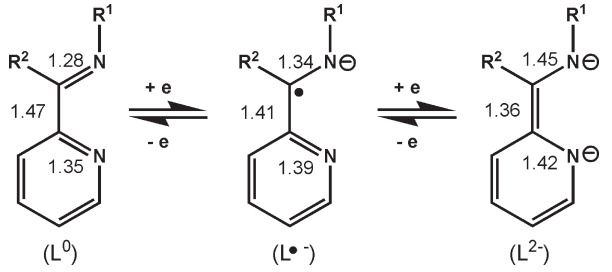

Assignments of the proton resonances were based on additional 2D COSY ^{1}H NMR data.

[(L^{2-})($L^{\bullet-}$)Co]Na(THF)$_6$ (1^{red}[Na(THF)$_6$]). The complex [($L^{\bullet-}$)$_2$Co] **1** (0.1908 g, 0.3225 mmol) was stirred overnight with 1.05 equiv of sodium metal (7.8 mg, 0.3393 mmol) in 10 mL of THF. The dark black-brown solution was evaporated under reduced pressure, and the resultant residue was rinsed with pentane (3 × 1 mL). The compound was characterized by a clean ^{1}H NMR spectrum and used without further purification. Yield: 0.208 g (60%). To obtain single crystals of X-ray quality, 1 equiv of 15-crown-5 was added to a concentrated THF solution of $\mathbf{1}^{red}$. Subsequent vapor diffusion of pentane into the solution afforded black hexagonal plates of $\mathbf{1}^{red}$[Na(15-crown-5)(THF)]. Elemental combustion results are consistent with $\mathbf{1}^{red}$[Na(15-crown-5)], likely because of loss of the THF molecule during the combustion experiment. Anal. Calcd for $C_{47}H_{67}CoN_4NaO_5$: C, 66.41; H, 7.95; N, 6.59. Found: C, 66.28; H, 8.10; N, 6.55. ^{1}H NMR (400 MHz, THF-d_8, 298 K): δ = 9.83 (dd, 2H, J = 2.8 and 5.2 Hz, pyridyl), 7.23 (t, 2H, J = 7.6 Hz, *p*-Ar), 7.11 (d, 4H, J = 7.6 Hz, *m*-Ar), 6.60 (s, 2H, imine C*H*), 6.13 (d, 2H, J = 2.8 and 6.8 Hz, pyridyl), 6.02 (m, 4H, pyridyl), 3.67 (m, obscured by THF, C*H*Me$_2$), 1.06 (d, 12H, J = 6.8 Hz, CH*Me*Me′), 0.87 (d, 12H, J = 6.8 Hz, CHMe*Me*′). ^{13}C NMR (100 MHz, THF-d_8, 300 K): δ = 159.6, 157.8, 146.5, 144.2, 126.5, 123.4, 123.0, 119.2, 117.1, 104.5, 28.5, 26.31, 26.27, 23.5.

[($L^{\bullet-}$)$_2$CoCH$_3$] (2). To a stirring THF solution of **1** (0.8390 g, 0.8058 mmol) was added 1 equiv of iodomethane (75.0 μL, 0.806 mmol) slowly dropwise. The solution immediately turned dark blue. After stirring for several hours, the solution was evaporated under reduced pressure. The resultant residue was rinsed with hexane, extracted with benzene, and filtered through Celite. After removing all solvents under reduced pressure, a dark blue powder was obtained. Single crystals of X-ray quality were grown by vapor diffusion of hexane into a benzene solution. Yield: 0.386 g (80%). Anal. Calcd for $C_{37}H_{47}CoN_4$: C, 73.24; H, 7.81; N, 9.23. Found: C, 73.25; H, 7.90; N, 9.30. ^{1}H NMR (400 MHz, THF-d_8, 300 K): δ = 8.80 (s, 2H, imine C*H*), 7.77 (d, 2H, J = 6.4 Hz, 6-pyridyl), 7.40 (d, 2H, J = 8.4 Hz, 3-pyridyl), 7.29 (d, 2H, J = 8.0 Hz, *m*-Ar), 7.20 (t, 2H, J = 7.6 Hz, *m*-Ar), 7.08 (ddd, 2H, J = 1.2, 6.8, and 8.0 Hz, 4-pyridyl), 6.91 (dd, 2H, J = 1.2 and 7.6 Hz, *p*-Ar), 6.69 (td, 2H, J = 1.2 and 6.4 Hz, 5-pyridyl), 2.50 (septet, 2H, J = 6.8 Hz, C*H*MeMe′), 2.44 (septet, 2H, J = 6.8 Hz, C′*H*MeMe′), 1.31 (d, 6H, J = 6.8 Hz, CH*Me*Me′), 1.16 (d, 6H, J = 6.8 Hz, CHMe*Me*′), 0.79 (d, 6H, J = 6.8 Hz, C′H*Me*Me′), 0.64 (s, 3H, CoCH_3), 0.37 (d, 6H, J = 6.8 Hz, C′HMe*Me*′). ^{13}C NMR (100 MHz, THF-d_8, 300 K): δ = 154.1, 152.7, 152.4, 145.7, 143.3, 141.5, 127.8, 125.9, 123.7, 123.2, 121.6, 115.5, 28.1, 27.9, 26.6, 25.7, 23.6, 21.7. All ligand-based ^{13}C resonances were found; but, the corresponding peak for CoMe was not observed. Substituting CH_3I with the labeled reagent $^{13}CH_3I$ in this preparation provided the labeled product [($L^{\bullet-}$)$_2$Co^{13}Me], which was then characterized by NMR spectroscopy. ^{1}H NMR (400 MHz, THF-d_8, 300 K): δ = 0.64 (d, ^1J(H, ^{13}C) = 130 Hz, Co*C*H$_3$). ^{13}C NMR (100 MHz, THF-d_8, 300 K): δ = 1.1 (Co*C*H$_3$). The NMR spectra were otherwise identical with those of the unlabeled analogue.

[($L^{\bullet-}$)$_2$CoI] (3). In a glass vessel [($L^{\bullet-}$)$_2$Co] **1** (0.2904 g, 0.4907 mmol) and 1 equiv of (*n*-Bu)$_3$SnI (0.156 mL, 0.491 mmol) were mixed in 5 mL of THF. After stirring overnight, the solution gradually changed color from dark brown to an intense royal purple. The solution was evacuated under reduced pressure until all the solvents were removed. The resultant residue was rinsed with pentane (3 × 1 mL) and dried under reduced pressure. The sample was then purified via crystallization involving vapor diffusion of pentane into either a benzene or a THF solution. The former was successful for growing single crystals of X-ray quality. Yield: 0.252 g (70%). Anal. Calcd for $C_{36}H_{44}CoIN_4$: C, 60.17; H, 6.17; N, 7.80. Found: C, 59.92; H, 6.15; N, 7.89. ^{1}H NMR (400 MHz, THF-d_8, 300 K): δ = 54.88 (br, imine C*H*), 20.69 (br, 6-pyridyl), 18.95 (br d, J = 4.8 Hz, 5-pyridyl), 15.34 (br d, J = 8.0 Hz, 3-pyridyl), 15.19 (br t, J = 7.2 Hz, 4-pyridyl), 7.06 (br d, J = 7.6 Hz, *m*-Ar), 6.71 (br d, J = 7.6 Hz, *m*-Ar), 5.08 (v br, C*H*MeMe′), 4.36 (br t, J = 7.6 Hz, *p*-Ar), 3.07 (v br, C′*H*MeMe′), 1.50 (CH*Me*Me′), 0.76 (C′H*Me*Me′), 0.56 (CHMe*Me*′), −0.42 (C′HMe *Me*′).

X-ray Crystallographic Data Collection and Refinement of the Structures. A black crystal of $\mathbf{1}^{red}$, a blue crystal of **2**, and a dark-brown crystal of **3** were coated with perfluoropolyether, picked up with nylon loops and mounted in the nitrogen cold stream of the diffractometer. A Bruker-Nonius Kappa-CCD diffractometer equipped with a Mo-target rotating-anode X-ray source and a graphite monochromator (Mo Kα, λ = 0.71073 Å) was used. Final cell constants were obtained from least-squares fits of all measured reflections. The structures were readily solved by direct methods and subsequent difference Fourier techniques. The Siemens ShelXTL[10] software package was used for solution and artwork of the structure, ShelXL97[11] was used for the refinement. All non-hydrogen atoms were refined anisotropically. Hydrogen atoms were placed at calculated positions and refined as riding atoms with isotropic displacement parameters. Crystallographic data of the compounds are listed in Table 1.

Physical Measurements. Electronic spectra of complexes were recorded with a Perkin-Elmer double-beam photometer (300 to 1700 nm). Cyclic voltammograms were recorded with an EG&G potentiostat/galvanostat. Variable temperature (2 to 350 K) magnetization data were recorded on a SQUID magnetometer (MPMS Quantum Design). The experimental magnetic susceptibility data were corrected for underlying diamagnetism using tabulated Pascal's constants. Simulations of magnetic susceptibility were carried out using the JulX program (version 13) written by Eckhard Bill. NMR spectra were recorded on Varian Mercury 400 MHz instruments at reported temperatures. For the VT experiments, a waiting time of 15 min was imposed prior to each collection to allow sufficient time for equilibration after each temperature increment (~10 K from 213 to 333 K).

Calculations. All calculations were done with the ORCA program package.[12] The geometry optimizations were carried out at the B3LYP level[13−15] of DFT. The all-electron Gaussian basis sets used were those reported by the Ahlrichs group.[16,17] For metal, nitrogen, oxygen, and iodine atoms, the triple-ζ-quality basis sets with one set of polarization functions were

(10) *SHELXTL*, version 6.12: Bruker AXS, 2001.
(11) Sheldrick, G. M. *SHELXL97*; University of Göttingen: Göttingen, Germany, 1997.
(12) Neese, F. *ORCA, an Ab Initio, Density Functional and Semiempirical Electronic Structure Program Package*, Version 2.6, Revision 4 ed.; Max-Planck-Institut für Bioanorganische Chemie: Mülheim/Ruhr, Germany, May 2005.
(13) Becke, A. D. *J. Chem. Phys.* **1993**, *98*, 5648.
(14) Becke, A. D. *J. Chem. Phys.* **1986**, *84*, 4524.
(15) Lee, C.; Yang, W.; Parr, R. G. *Phys. Rev. B* **1988**, *37*, 785.
(16) Schäfer, A.; Huber, C.; Ahlrichs, R. *J. Chem. Phys.* **1994**, *100*, 5829.
(17) Schäfer, A.; Horn, H.; Ahlrichs, R. *J. Chem. Phys.* **1992**, *97*, 2571.

Table 1. Crystallographic Data for $\mathbf{1}^{red}$, **2**, and **3**

	[$\mathbf{1}^{red}$]Na(15-crown-5)THF	0.974[**2**]·0.026[**3**]	**3**
chemical formula	$C_{50}H_{72}N_4O_6CoNa$	$C_{36.97}H_{46.92}N_4CoI_{0.03}$	$C_{36}H_{44}CoIN_4$
crystal size, mm^3	0.24 × 0.21x 0.15	0.30 × 0.30 × 0.20	0.06 × 0.05 × 0.04
F_W	907.04	609.51	718.58
space group	$P2_1/n$, No. 14	$C2/c$, No. 15	$P2_1/c$, No. 14
a, Å	10.1252(3)	21.503(2)	15.692(2)
b, Å	35.722(1)	9.8022(9)	10.267(1)
c, Å	13.8017(4)	17.244(1)	22.037(2)
α, deg	90	90	90
β, deg	102.775(3)	114.022(3)	108.987(2)
γ, deg	90	90	90
V, Å	4868.4(3)	3319.7(5)	3357.2(6)
Z	4	4	4
T, K	100(2)	100(2)	100(2)
ρ calculated, g cm^{-3}	1.238	1.220	1.422
refl. collected/$2\Theta_{max}$	106597/60.0	31290/66.36	120507/70.12
unique refl./$I > 2\sigma(I)$	14193/10658	6319/5555	14830/12887
no. params./restraints	567/0	198/1	387/0
λ, Å /μ(Kα), cm^{-1}	0.71073/4.12	0.71073/5.71	0.71073/14.61
R1[a]/ goodness of fit[b]	0.0450/1.032	0.0353/1.021	0.0199/1.051
wR2[c] ($I > 2\sigma(I)$)	0.0971	0.0850	0.0497
residual density, e Å^{-3}	+0.693/−0.481	0.634/−0.794	0.826/−0.507

[a] Observation criterion: $I > 2\sigma(I)$. $R1 = \sum||F_o| - |F_c||/\sum|F_o|$. [b] $GOF = [\sum[w(F_o^2 - F_c^2)^2]/(n-p)]^{1/2}$. [c] $wR2 = [\sum w(F_o^2 - F_c^2)^2/\sum w(F_o^2)^2]^{1/2}$ where $w = 1/\sigma^2(F_o^2) + (aP)^2 + bP$, $P = (F_o^2 + 2F_c^2)/3$.

used (TZVP).[16] The carbon and hydrogen atoms were described by smaller polarized split-valence SV(P) basis sets (double-ζ-quality in the valence region with a polarizing set of d-functions on the non-hydrogen atoms).[17] The SCF calculations were tightly converged (1×10^{-8} Eh in energy, 1×10^{-7} Eh in the density change, and 1×10^{-7} in the maximum element of the DIIS error vector). The geometries were considered converged after the energy change was less than 5×10^{-6} Eh, the gradient norm and the maximum gradient element were smaller than 1×10^{-4} and 3×10^{-4} Eh/Bohr, respectively, and the root-mean-square and maximum displacements of the atoms were smaller than 2×10^{-3} and 4×10^{-3} Bohr, respectively. Solvation effects were included using the conductor-like screening model (COSMO).[18] In these cases, the solvent THF was modeled with a dielectric constant of 7.25 and a refractive index of 1.407.

III. Results

Synthesis and Spectroscopic Characterization of $\mathbf{1}^{red}$. Previously, we reported that the neutral bis(iminopyridine)cobalt complex (**1**) contains two monoanionic π^* radicals ($L^{\bullet-}$). The cyclic voltammogram of complex **1** showed three reversible redox events at −0.76, −1.26, and −1.96 V (vs Fc+/Fc, 0.1 M [N(*n*-Bu)$_4$]PF$_6$ in THF).[4] The two anodic peaks were assigned as ligand-based oxidations. Subsequently, the first oxidation product was prepared and characterized as the THF-adduct [($L^{\bullet-}$)(L^0)Co(THF)]B(Ar$_F$)$_4$ ([$\mathbf{1}^{ox}$·THF]B(Ar$_F$)$_4$), where Ar$_F$ = 3,5-(CF$_3$)$_2$(C$_6$H$_3$).

Our recent efforts were directed at understanding the cathodic peak at −1.96 V and exploring the reactivity profile of this reduced species. By stirring a THF solution of **1** over sodium metal, the singly reduced form was cleanly generated as the sodium salt [$\mathbf{1}^{red}$]Na(THF)$_6$ as shown in Scheme 2. Complex $\mathbf{1}^{red}$ is diamagnetic. In its ^{1}H NMR spectrum at rt, only a single resonance is observed for each chemically different proton with the exception of the methyl group, for which two peaks are observed (0.87 and 1.06 ppm) (see Supporting Information, Figure 1). Thus in solution, the two ligands must be related by symmetry. Slow rotation of the N—C$_{ipso}$ bond in the 2,6-diisopropylphenyliminyl group would generate distinct methyl resonances. However, the observation of two peaks rather than four suggests that two sets of methyl groups on one ligand are equivalent by symmetry, that is, a mirror plane. The two possible orientations for this case are illustrated in Scheme 3a, wherein the methyl groups are either pointed toward or away from the cobalt center.

Scheme 2. Syntheses of $\mathbf{1}^{red}$, **2**, and **3**

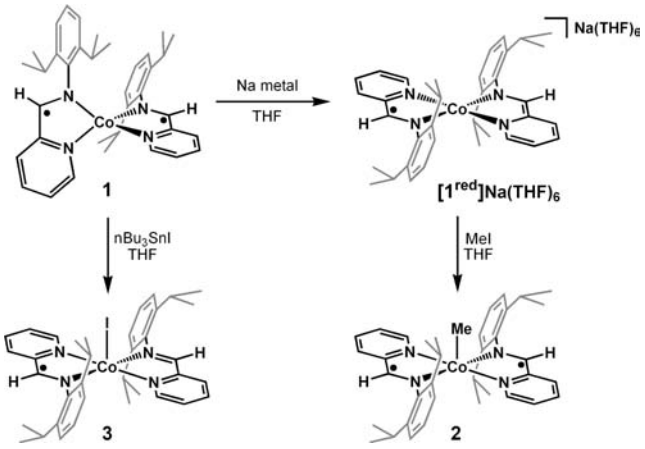

Complex $\mathbf{1}^{red}$ represents the third isolated complex in the electron-transfer series that includes **1** and $\mathbf{1}^{ox}$. Figure 1 is an overlay of their electronic absorption spectra. All three members are dark brown, although **1** and $\mathbf{1}^{red}$ are significantly more intense in color compared to $\mathbf{1}^{ox}$. Indeed, the UV−vis/NIR region for **1** and $\mathbf{1}^{red}$ are similar, but only until 900 nm. Unlike **1**, $\mathbf{1}^{red}$ possesses an additional adsorption band in the NIR region at 1086 nm with a large extinction coefficient (ε) of 11,600 M^{-1} cm^{-1}. In the latter respect, $\mathbf{1}^{red}$ is more akin to $\mathbf{1}^{ox}$, which also displays a NIR band at 1077 nm with ε = 3,900 M^{-1} cm^{-1}

(18) Sinnecker, S.; Rajendran, A.; Klamt, A.; Diedenhofen, M.; Neese, F. *J. Phys. Chem. A* **2006**, *110*, 2235.

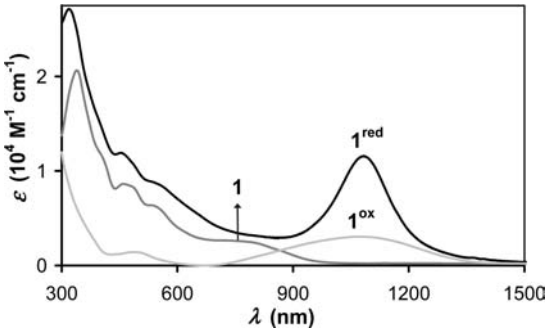

Figure 1. Electronic absorption spectra of $\mathbf{1}^{red}$ in THF, **1** in benzene, and $\mathbf{1}^{ox}$ in THF.

Table 2. Electronic Spectra[a] of Complexes in THF[b] at 22 °C

complexes	λ_{max}, nm (ε, 10^3 M^{-1} cm^{-1})
$\mathbf{1}^{red}$	319 (27), 454 (12), 534 sh, 1086 (12)
1	335 (21), 400 sh, 450, 475 (8.5), 535 sh, 790 (3.2)
$\mathbf{1}^{ox}$	485 (1.4), 1077 (3)
2	360 sh, 494 (6.1), 626 (8.3), 870 (12)
3	360 sh, 487 (5.0), 750 sh, 935 (9.5)

[a] Data for **1** and $\mathbf{1}^{ox}$ were previously reported. See ref 4. [b] With one exception, **1** is in C_6H_6.

Scheme 3. Different Chemical Environments of the Methyl Groups in the Ligand with Slow Rotation about the N—C(ipso) Bond and (a) with the Presence or (b) Absence of the Mirror Plane As Drawn

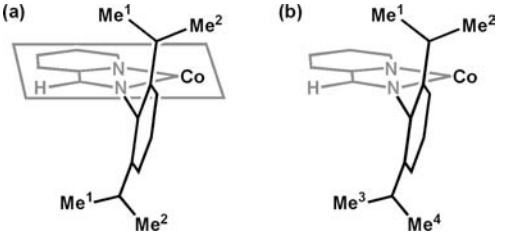

(Table 2). Both of these NIR bands are proposed to be intervalence charge transfer bands because of their high intensities and low energies (vide infra). Previously, we interpreted the IVCT band exhibited by $\mathbf{1}^{ox}$ as characteristic of a fully delocalized Class III ligand-mixed-valent complex, wherein the formal oxidation states of the two ligands in $\mathbf{1}^{ox}$ are the monoanionic ($L^{\bullet -}$) and the neutral (L^0) states.[19,20] The similarity of the NIR absorption exhibited by $\mathbf{1}^{red}$ strongly suggests that it is also a ligand-based IVCT. Since the experimental bandwidth at half intensity (3590 cm^{-1}) is much lower than the theoretical value calculated using Hush's equation (4630 cm^{-1}),[21] the designation of $\mathbf{1}^{red}$ as a Class III ligand-mixed-valent complex is suitable. It is unlikely that the formal ligand oxidation states in $\mathbf{1}^{ox}$ and $\mathbf{1}^{red}$ are similar given that the two complexes differ by two electrons. Instead, we propose that the formal ligand oxidation states in $\mathbf{1}^{red}$ are the monoanionic ($L^{\bullet -}$) and the dianionic (L^{2-}) states.

(19) Creutz, C. In *Prog. Inorg. Chem.*; Lippard, S. J., Ed.; Wiley: New York, 1983; Vol. *30*, p 1.
(20) Robin, M. B.; Day, P. *Adv. Inorg. Chem. Radiochem.* **1967**, *10*, 247.
(21) Hush, N. S. In *Prog. Inorg. Chem.*; Cotton, F. A., Ed.; Interscience: New York, 1967; Vol. *8*, p 391.

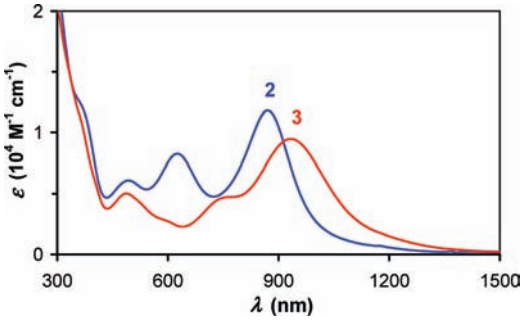

Figure 2. Electronic absorption spectra of **2** (blue) and **3** (red) in THF.

Thus, our proposal for the electron-transfer series is

$$[Co^{II}(L^{\bullet -})(L^0)(THF)]^{1+} \overset{E^{o\prime}_{+/0}}{\underset{-e}{\overset{+e}{\rightleftharpoons}}} [Co^{II}(L^{\bullet -})_2]^0 \overset{E^{o\prime}_{0/-}}{\underset{-e}{\overset{+e}{\rightleftharpoons}}} [Co^{II}(L^{\bullet -})(L^{2-})]^{1-}$$

$\mathbf{1}^{ox}$•THF **1** $\mathbf{1}^{red}$

Syntheses and Spectroscopic Characterizations of 2, 3. The electron-rich $\mathbf{1}^{red}$ reacts immediately with iodomethane in THF to give a dark blue solution (Scheme 2). By ^{1}H NMR spectroscopy, the predominant product is diamagnetic and is consistent with a methylcobalt complex (**2**) because of a signature peak at 0.64 ppm that integrates to three protons and shows no J-coupling. The presence of only one resonance for the iminyl proton and the pyridyl protons is consistent with the two iminopyridines being chemically equivalent. However, the total number of resonances in the ^{1}H NMR spectrum is greater for **2** than for $\mathbf{1}^{red}$ (Supporting Information, Figure 2). The additional peaks arise from inequivalent protons in the diisopropylphenyl functionality: the meta hydrogens of the aryl ring and the methine hydrogens of the isopropyl groups are now distinct, and four different methyl peaks are observed. This scenario requires (1) slow rotation of the N—C_{ipso} bond and (2) a low symmetry environment such as that depicted in Scheme 3b.

The ^{1}H NMR spectra of crude samples of **2** consistently revealed a trace amount of an impurity, which was suspected to be the analogous iodocobalt species **3**. Generating a clean batch of the iodocobalt complex for comparison proved nontrivial. Combining $\mathbf{1}^{red}$ with I_2, ICl, *N*-iodosuccinimide, or KI_3 resulted in mixtures of the supposed iodocobalt species and **1**. Indeed, a competing side reaction would be outer-sphere electron-transfer from $\mathbf{1}^{red}$ to the oxidizing reagent and consequently producing **1**. The alternative strategy of using **1** instead of $\mathbf{1}^{red}$ and an I• source such as tributyltin iodide was successful in providing a clean sample of the iodocobalt complex **3**, whose identity was confirmed by a single crystal X-ray diffraction study (vide infra).

The electronic spectra of **2** and **3** are shown in Figure 2 with maxima listed in Table 2. Notably, a NIR absorption band is observed for both **2** and **3** at close energies and with similar intensities (**2**: 870 nm or 11,494 cm^{-1}, ε = 11,800 M^{-1} cm^{-1}; **3**: 935 nm or 10,695 cm^{-1}, ε = 9,500 M^{-1} cm^{-1}). In contrast, the ^{1}H NMR spectra of the two complexes are quite dissimilar. The VT ^{1}H NMR spectrum of **3** in THF-d_8 from 213 to 333 K is shown in Figure 3, wherein the peak assignments were deduced from a 2D COSY NMR experiment (Supporting

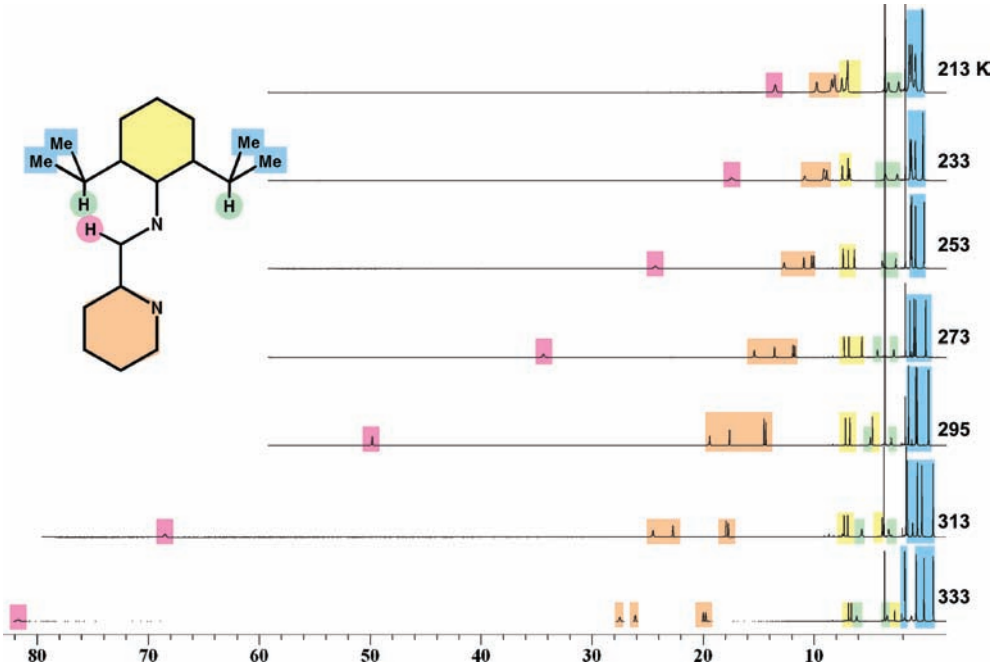

Figure 3. Variable-temperature ^{1}H NMR of **3** in THF-d_8 from 213 to 333 K.

Information, Figure 3). While **2** exhibits a diamagnetic spectrum that is virtually invariant from −20 to 40 °C, the peaks corresponding to **3** have a wide range from −0.5 to 55 ppm at 295 K. Lowering the temperature to −60 °C significantly reduces this range to within 0 and 15 ppm. Conversely, raising of the temperature to +60 °C results in a larger spread from −1 to 82 ppm. Interestingly, all the protons in the plane of the ligand backbone including the pyridyl ring shift grossly downfield (Δ > 12 ppm) at 333 K versus 213 K. This is especially true of the iminyl proton, which moves by nearly 70 ppm. The other ligand protons show smaller positional changes, but certain trends can be drawn. For example, all the aryl protons of the diisopropylphenyl group move slightly upfield with increasing temperature, with the para proton evincing the most notable change, Δ = −4.3 ppm. On the other hand, the methine protons shift downfield with overall displacements of +2.8 and +1.0 ppm. The methyl resonances neither shifted significantly nor shifted in the same direction.

If complex **3** is a paramagnet, then the range in chemical shifts are expected to increase with decreasing temperature. Because the completely opposite trend is observed here, the paramagnetic shifts at high temperatures indicate a thermal equilibrium between a paramagnetic excited state and a diamagnetic ground state of **3**.[22] Incidentally, we have also examined if the signals display Curie behavior in that the isotropic shifts vary linearly with inverse temperature (Supporting Information, Figure 4).[23] No linear relationship was found, but this is not surprising since deviation from overall Curie behavior was already observed in the magnetic susceptibility

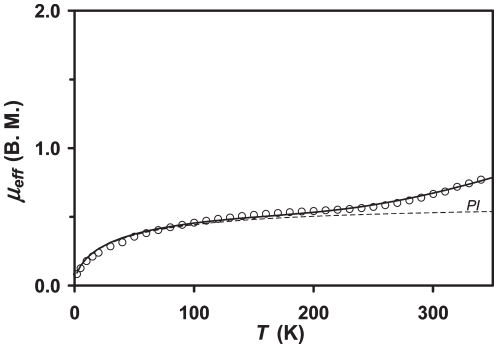

Figure 4. Temperature dependence of the magnetic moment, μ_{eff} of **3** (shown in open circles). The solid line represents the best fit, which includes a small percentage of a paramagnetic impurity (PI). The data was corrected for χ_{TIP} of 1.194 × 10^{-3} emu. See text for simulation parameters.

study of **3** (vide infra). Although we could not parametrize the contact and dipolar terms, it is telling that all the protons in the ligand backbone shifted downfield. In paramagnetic complexes wherein all the ligand protons shift to one direction, one normally assumes that delocalization of the paramagnetic spin into the ligand atoms occurs by direct spin delocalization, and the magnitude of the shifts is expected to drop off with increasing number of bond(s) from the metal center.[24] Indeed for **3**, the two most shifted protons, the iminyl and the 6-pyridyl protons, are the nearest to the cobalt center with only three intervening bonds each. However, the discrepancy in magnitude between the shifts of the 6-pyridyl proton and the iminyl proton (70 versus 20 ppm) suggest that spin-delocalization is not the only operating mechanism. We presume that the local spin density on the ligands, which by interacting with the spin density at the metal

(22) Jesson, J. P. In *NMR of Paramagnetic Molecules*; La Mar, G. N., Horrocks, W. D., Jr., Holm, R. H., Eds.; Academic Press: New York, **1973**; p 41.

(23) Holm, R. H.; Hawkins, C. J. In *NMR of Paramagnetic Molecules*; La Mar, G. N., Horrocks, W. D., Jr., Holm, R. H., Eds.; Academic Press: New York, **1973**, p 316.

(24) Ming, L.-J. In *Physical Methods in Bioinorganic Chemistry: Spectroscopy and Magnetism*; Que, L., Jr., Ed.; University Science Books: Sausalito, CA, **2000**; p 375.

center, could also affect chemical shifts. Thus, the much greater spin density at the iminyl carbon versus the 2-pyridyl carbon may give rise to the large difference in the shifts of their attached protons.

Magnetic Susceptibility Measurements of 3. The temperature-dependent paramagnetism of the iodocobalt complex was further investigated by measuring the magnetic susceptibility of solid **3** in an applied field of 7.0 T. The large applied field was chosen to mimic the field strength of the ^{1}H NMR studies (400 MHz, 9.4 T). The plot of μ_{eff} versus T is shown in Figure 4 over the temperature range 2 to 350 K. The magnetic moment μ_{eff} increases gradually from 0.08 μ_B at 2 K to 0.74 μ_B at 359 K, which is well below the value of 1.73 μ_B for a single unpaired electron. Thus, the main magnetic response is attributed to a paramagnetic impurity (assuming high-spin Co(II), $S = 3/2$, 2.4%) even though the sample was assessed as pure by elemental analysis.

Notably, the paramagnetic impurity cannot account for the small rise of μ_{eff} from 0.55 to 0.74 μ_B in the high temperature regime, 250 to 350 K. In conjunction with our VT NMR results, we believe that this small rise reflects the onset of a Boltzmann population of an energetically low-lying excited state. Imposing a two-spin model comprising a metal and a ligand-based spin with $S_{Co} = S_L = 1/2$, the spectra can be well-simulated by adopting $g_{Co} = 2.13$, $g_L = 2.00$ (set), and a strong antiferromagnetic isotropic spin coupling constant, $J = -535$ cm^{-1} for the Hamiltonian $\hat{H} = -2J\hat{S}_{Co}\cdot\hat{S}_L$. Because of the small magnetic response, there is flexibility in these fit values. Alternative simulations provide g_1 values as high as 2.33 and J of -550 cm^{-1}, implying that g_1 cannot be determined, but a ballpark estimate of -500 cm^{-1} for the coupling constant is probably reasonable. The onset of an excited state resulting from an "uncoupling" of a metal and ligand-centered electron have been observed in other coordination complexes featuring ligand radicals,[25] including a recent example of an iron (III) center stabilized by three open-shell diketone-type ligands.[26]

Solid-State Structures. The molecular structures for $\mathbf{1}^{red}$, **2**, and **3** have been determined by single crystal X-ray diffraction studies at 100 K and are shown in Figures 5, 6, and 7, respectively. Crystallographic details are provided in Table 1, and relevant geometrical parameters are listed in Table 3. In our hands, complex $\mathbf{1}^{red}$ was only successfully crystallized using 15-crown-5 ether to encapsulate the sodium ion as [Na(15-crown-5)THF]. Complex $\mathbf{1}^{red}$ is a distorted tetrahedron with an angle between the two metal−ligand planes (θ) of 26.88(5)°. In this regard, $\mathbf{1}^{red}$ resembles more a distorted square plane since previous four-coordinate bis(iminopyridine)metal complexes displayed angles that range from 71 to 84°. For instance, the angle in the neutral analogue **1** is 80(1)°. In the structure of $\mathbf{1}^{red}$, the iminyl nitrogens are *trans* to one another, likely because of steric repulsion between the two bulky diisopropylphenyl groups. An approximate C_2 axis of symmetry passes through the cobalt center, equalizing the two ligands, which is consistent with the ^{1}H NMR spectrum. However, there is no mirror plane in the static structure of $\mathbf{1}^{red}$ as suggested in Scheme 3 to rationalize the presence of only two methyl types in the ^{1}H NMR spectrum. If, however, the two metal−ligand planes are rapidly twisting between θ and $-\theta$ (through $\theta = 0$) in solution, then the methyl groups above and below the ligands planes become equivalent as if a mirror plane was present.

Penta-coordinate **2** and **3** are nearly isostructural in their solid-state structures, with θ of 49.58(4)° and 48.16 (3)°, respectively. In **2**, a C_2 axis coincides perfectly with

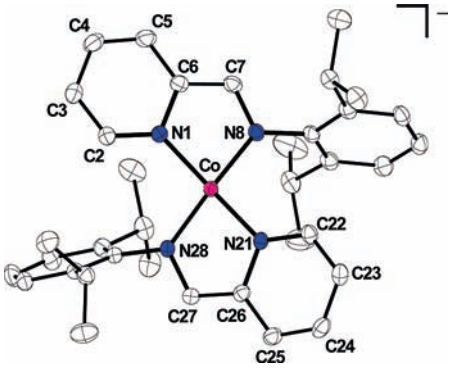

Figure 5. Thermal ellipsoid representation (50%) of complex [$\mathbf{1}^{red}$]Na (15-crown-5)(THF). Hydrogen atoms and counterion have been omitted.

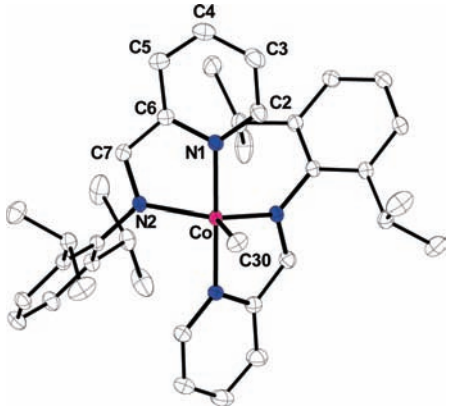

Figure 6. Thermal ellipsoid representation (50%) of complex **2**. Hydrogen atoms have been omitted.

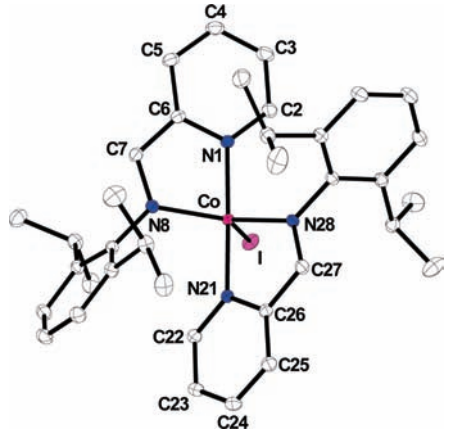

Figure 7. Thermal ellipsoid representation (50%) of complex **3**. Hydrogen atoms have been omitted.

(25) Chaudhuri, P.; Verani, C. N.; Bill, E.; Bothe, E.; Weyhermüller, T.; Wieghardt, K. *J. Am. Chem. Soc.* **2001**, *123*, 2213.

(26) Spikes, G. H.; Bill, E.; Weyhermüller, T.; Wieghardt, K. *Angew. Chem., Int. Ed.* **2008**, *47*, 2973.

Table 3. Comparison of Experimental and Theoretical Bond Distances (Å) and Angles (deg) in Complexes $\mathbf{1}^{red}$, **2**, and **3**

	$\mathbf{1}^{red}$		**2**			**3**	
BS(*n*,*m*)	exp	BS(1,1)	exp	BS(1,1)	BS(2,2)	exp	BS(1,1)
Co−X			*2.048(2)*	1.985	2.013	*2.6311(3)*	2.744
$Co-N_{imine}$	*1.877(1)*	1.934	*1.9025(7)*	1.983	2.011	*1.9029(8)*	2.005
Co−N8, Co−N28	*1.874(1)*					*1.9077(7)*	2.011
$Co-N_{pyridine}$	*1.898(1)*	1.962	*1.9139(8)*	1.957	1.961	*1.9279(8)*	1.961
Co−N1, Co−N21	*1.905(1)*					*1.9337(8)*	
C−C′	*1.381(2)*	1.387	*1.411(1)*	1.414	1.416	*1.423(1)*	1.427
C6−C7, C27−C28	*1.376(2)*					*1.423(1)*	
$C-N_{imine}$	*1.360(2)*	1.372	*1.333(1)*	1.333	1.334	*1.323(1)*	1.313
C7−N8, C27−N28	*1.366(2)*					*1.321(1)*	1.316
$C'-N_{pyridine}$	*1.404(2)*	1.407	*1.377(1)*	1.382	1.381	*1.368(1)*	1.372
C6−N1, C26−N21	*1.406(2)*					*1.360(1)*	
θ^a	*26.88(5)*	34.07	*49.58(4)*	37.23	58.29	*48.16(3)*	38.15

[a] Theta is the angle between the two metal−ligand planes.

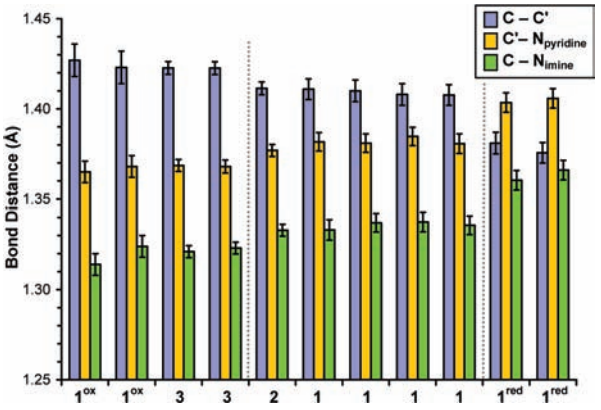

Figure 8. Plotted individual bond distances (Å, ± 3 esd) of all the ligand backbones in the cobalt series: C−C′ (blue), C′-$N_{pyridine}$ (yellow), and C−N_{imine} (green), in order of decreasing C−C′ values.

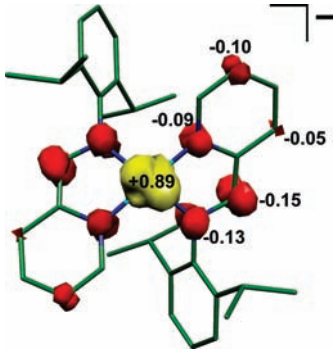

Figure 9. Spin density plot of the calculated monoanion $\mathbf{1}^{red}$ shown with values based on a Mulliken spin population analysis. Numerical values of spin densities are shown for only one ligand (the two ligands have equivalent spin densities), and only atoms with |spin densities| ≥ 0.05 are labeled. The spin densities over both ligands sum to −0.89.

the Co−Me vector, so that the two iminopyridines are absolutely equivalent within the crystal. In **3**, this C_2 axis is only approximate with the Co−I vector, as is consistent with its ^{1}H NMR spectra. Both **2** and **3** are distorted trigonal bipyramids, wherein the pyridyl nitrogens are nearly axial (179.08(4)° and 174.85(3)° respectively) and the iminyl nitrogens lie in the equatorial plane: the sum of $N_{imine}-Co-N_{imine}'$, $N_{imine}-Co-X$, and $N_{imine}'-Co-X$ angles is 360.00(4)° and 360.01(2)° for **2** and **3**, respectively (X = Me, I). Twisting of the two metal−ligand planes between θ and $-\theta$ is improbable since it would require the dissociation of the X ligand. This limited rotation leads to a lower overall symmetry for **2** and **3** compared to $\mathbf{1}^{red}$, which is consistent with their NMR spectra.

Of particular interest are the perturbations in the ligand backbone bond distances, which are depicted as a column plot (Figure 8) along with bond lengths previously reported for **1** and $[\mathbf{1}^{ox}\cdot THF]B(Ar_F)_4$. According to Scheme 1, changes in the ligand oxidation state by one electron are marked by bond changes in the ligand backbone of about half a bond order. The mere half-bond order difference is due to the delocalization of the electron density in the ligand π,π^* framework. This situation becomes complicated in bis(ligand)metal complexes, wherein the electron density of one electron can be delocalized over both ligands. In the case of full delocalization, only a quarter a bond order change is expected. Given the inherent difficultly in distinguishing such a small bond order change, we present our full collection of cobalt complexes featuring this ligand. Each column in Figure 8 represents a unique ligand bond distance from X-ray crystallography data with errors of ± 3 esd.

Notably, the ligands are practically equivalent within each cobalt complex. The data also suggests three distinct categories of ligand oxidation states. Previously, **1** was shown to consist of two ligand radicals ($L^{\bullet-}$), whereas $\mathbf{1}^{ox}$ was formally mixed-valent featuring delocalized ($L^{\bullet-}$) and (L^0) states. Surprisingly, complex **2** and **3** seem to belong to different categories. Complex **3** is formally mixed-valent featuring a divalent metal center and a single ligand radical, $(L^{\bullet-})(L^0)Co^{II}I$. In contrast, complex **2** is better described as possessing a trivalent metal center with two ligand radicals, $(L^{\bullet-})_2Co^{III}Me$. Finally, complex $\mathbf{1}^{red}$ represents another class, which is formally mixed-valent comprising a fully reduced ligand (L^{2-}) and a single ligand radical ($L^{\bullet-}$).[27,28] This interpretation lends support to the observation of a ligand−ligand IVCT band for $\mathbf{1}^{ox}$ and $\mathbf{1}^{red}$ but not for **1**, in which a ligand-to-ligand transition must be accompanied by a spin-state change and is thus spin-forbidden.

(27) Khusniyarov, M. M.; Bill, E.; Weyhermüller, T.; Bothe, E.; Harms, K.; Sundermeyer, J.; Wieghardt, K. *Chem.—Eur. J.* **2008**, *14*, 7608.
(28) Hess, C. R.; Weyhermüller, T.; Bill, E.; Wieghardt, K. *Angew. Chem., Int. Ed.* **2009** *48*, 3703.

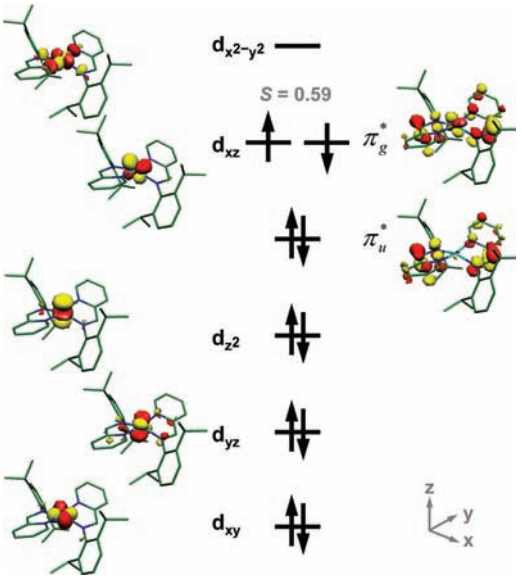

Figure 10. Qualitative MO diagram of the magnetic orbitals derived from the BS(1,1) calculation of the monoanion $\mathbf{1}^{red}$. The spatial overlap (S) of the corresponding alpha and beta orbitals are provided for the case when $S \neq 1.0$.

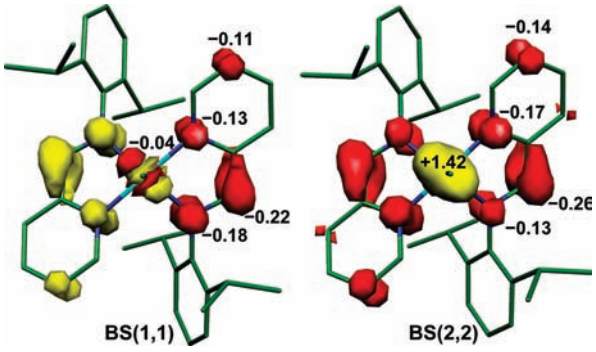

Figure 11. (left) Spin density plot of the BS(1,1)-calculated **2**. The two ligands have spin density values of +0.71 and −0.75. (right) Spin density plot of the BS(2,2)-calculated **2**. Both ligands have total spin density values of −0.76 each.

DFT Calculations. The geometry of $\mathbf{1}^{red}$, **2**, and **3** have been optimized using DFT calculations at the B3LYP level. The calculated geometries are given in Table 3 alongside their experimental values. Broken-symmetry calculations are denoted by the label BS(x,y), which represents a broken-symmetry state of x spin-up electrons and y spin-down electrons.[29,30] The x and y electrons can be localized in different parts of the molecule, that is, they are not forcibly paired. All complexes were calculated as spin singlets $S = 0$, and initial atom coordinates were taken from their solid-state structures. Overall, the calculated geometrical parameters reproduce the experimental values well. All ligand-backbone bond distances are within ± 0.01 Å.

The spin density plot and molecular orbital (MO) splitting diagram of calculated $\mathbf{1}^{red}$ is shown in Figures 9 and 10, respectively. Both depictions are consistent with an electronic structure consisting of a low-spin Co(II) center ($S_{Co} = 1/2$) that is coupled antiferromagnetically to a single electron that is delocalized over the gerade π^* molecular orbital of the two ligands. Hence, the proposed electronic structure of $\mathbf{1}^{red}$ as the Class III ligand mixed-valent species $[(L^{\bullet -})(L^{2-})Co^{II}]^{-}$ is compatible with the DFT results.

Interestingly, two viable solutions are found for **2**: a BS (1,1) and a BS(2,2) state. The two solutions for **2** are practically isoenergetic; the BS(1,1) state is predicted to be lower in energy by only 1.09 kcal/mol. Both of these calculated structures reproduce the ligand bond parameters well. However, both have slightly deviant θ's

(29) Noodleman, L. *J. Chem. Phys.* **1981**, *74*, 5737.
(30) Noodleman, L.; Davidson, E. R. *Chem. Phys.* **1986**, *109*, 131.

Table 4. Reduced d-Orbital Charges and Spin Densities of the Broken-Symmetry DFT-Calculated Structures of **2**

	BS(1,1)			BS(2,2)		
	charge	spin	population	charge	spin	population
$d_{x^2-y^2}$	0.73	0.03	0	0.83	0.18	0
d_{z^2}	0.96	0.38	0 (↑)[a]	1.51	0.36	↑ (↑↓)[a]
d_{xz}	1.94	0.03	↑↓	1.20	0.73	↑
d_{yz}	1.94	0.02	↑↓	1.94	0.01	↑↓
d_{xy}	1.94	0.01	↑↓	1.94	0.02	↑↓

[a] Alternative interpretations are included in parentheses.

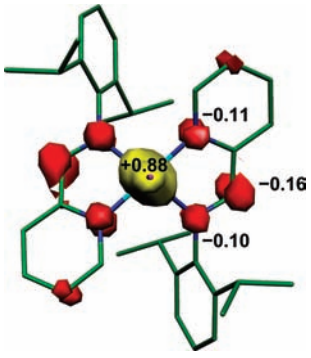

Figure 12. Spin density plot of calculated **3**. The total spin density for both ligands is −0.93, with a spin density of 0.05 on I.

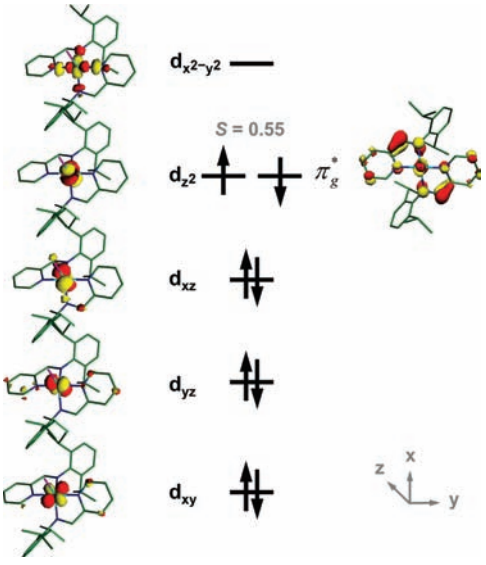

Figure 13. Qualitative MO diagram of the magnetic orbitals derived from the BS(1,1) calculation of **3**. The spatial overlap (S) of the corresponding alpha and beta orbitals are provided for the case when $S \neq 1.0$.

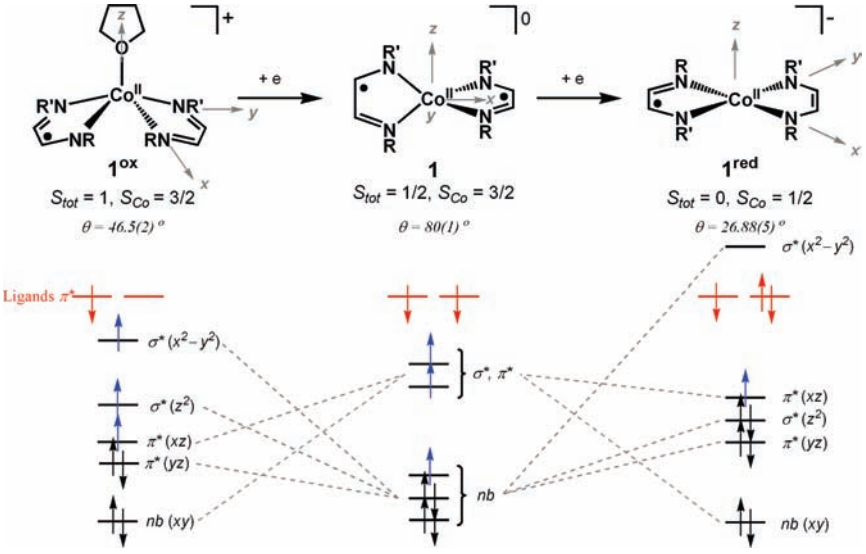

Figure 14. Summary of the electron-transfer series comprising $\mathbf{1}^{ox}\cdot$THF, **1**, and $\mathbf{1}^{red}$. Qualitative d-orbital splitting diagrams reveal the consequences of the structural changes with the addition (or removal) of electrons. Note that the x,y,z-axes in **1** are rotated ~45° relative to that in $\mathbf{1}^{ox}\cdot$THF and $\mathbf{1}^{red}$.

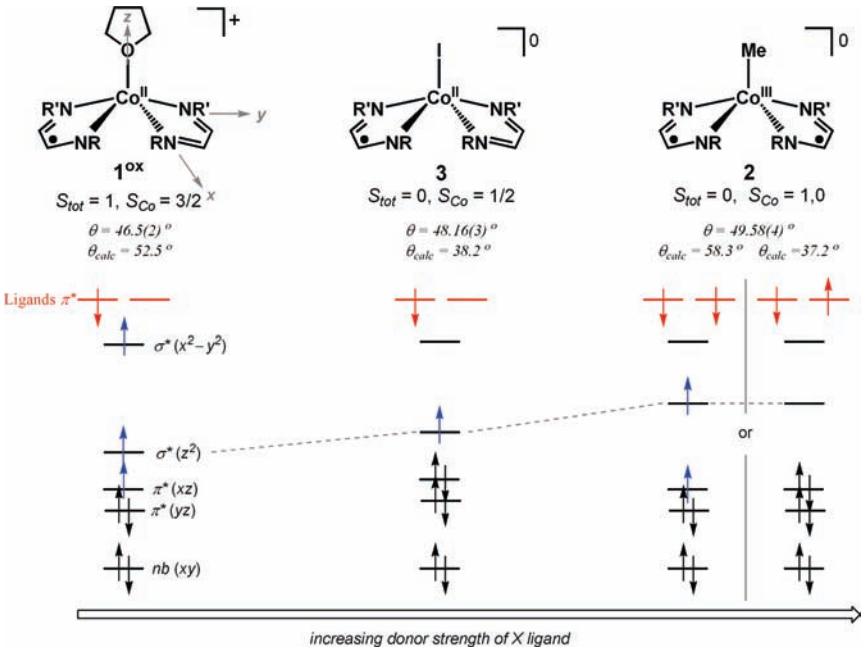

Figure 15. Summary of the 5-coordinate bis(iminopyridine)cobalt series comprising $\mathbf{1}^{ox}\cdot$THF, **2**, and **3**. Qualitative d-orbital splitting diagrams reveal the consequences of altering the X ligand. Coordinate axes are the same in this series and are shown superimposed on $\mathbf{1}^{ox}\cdot$THF.

albeit in different directions. The spin density plots of the two calculated variants of **2** are displayed in Figures 11. At first glance, one would suppose the two solutions to represent an electronic structure featuring two ligand radicals and a Co(III) center, whereby the differences between the BS(1,1) and BS(2,2) solutions are the low-spin versus intermediate-spin metal configuration, respectively, and the antiferromagnetic versus ferromagnetic coupling of the two ligand radicals, respectively. Unfortunately, this simplistic picture is inaccurate as the absolute value of the spin density per ligand sums to only ~0.76 electron on average, and the corresponding spin density on cobalt in the BS(2,2) state is a non-integer value of 1.42.

Recently, Khusniyarov et al. described an approach to deduce the electronic structure in ambiguous cases by analyzing the reduced charges and spin densities of each individual d-orbital.[31] We employ this strategy here, and the reduced d-orbital charges and spin densities of the two calculated structures of **2** are collected in Table 4. A d-orbital with a charge of 2 and zero spin is clearly doubly occupied (denoted by ↑↓). Along this line of reasoning, a singly occupied orbital should have both charge and spin values of 1, and an empty orbital is reflected by zero values. Deviations from the expected values are observed and are attributed to covalency between metal and ligand-based orbitals. Such covalency can perturb the expected values by transferring charge and spin (i.e., spin-polarization) from ligand-to-metal and vice versa.

(31) Khusniyarov, M. M.; Weyhermüller, T.; Bill, E.; Wieghardt, K. *J. Am. Chem. Soc.* **2009**, *131*, 1208.

Nonetheless, the authors have stipulated that a reduced spin density >0.5 may be interpreted as a single unpaired electron, whereas a spin density <0.5 signifies either double or no occupation. The latter two possibilities would then be easily distinguished by the corresponding reduced orbital charge.

The occupancy of the d-orbitals is fairly straightforward in either the BS(1,1) or the BS(2,2) calculation of **2**, with the exception of the d_{z^2} orbital (Table 4). The d_{z^2} orbital is energetically high-lying because of its sigma-antibonding interaction with the methyl group. Though we favor the Co (III) electronic structure ($S_{Co} = 0$) in conjunction with the X-ray structural results, there is the possibility of an alternative interpretation featuring Co(II), $S_{Co} = 1/2$. In summary, no clear electronic picture emerges from our DFT studies of **2**. The DFT results suggest a borderline case between Co(III) with two ligand radicals and a Co(II) electronic structure with one ligand radical.

Various broken-symmetry optimizations of **3** all converged to a single solution, namely BS(1,1). A spin-density plot of calculated **3** is shown in Figure 12. The local spin densities agree nicely with an unpaired electron on cobalt, which is coupled antiferromagnetically to a single unpaired electron that is delocalized over the two ligands. The MO diagram of **3** (Figure 13) establishes the electronic structure of **3** as formally $[(L^{\bullet-})(L^0)Co^{II}I]$ comprising a low-spin Co(II) center and two mixed-valent ligands with a fully delocalized ligand radical. Interestingly, the electronic picture of calculated **3** is isoelectronic with the alternative one proposed for **2**.

IV. Conclusion

We report three new cobalt coordination complexes featuring the redox-active α-iminopyridine. With the isolation of $\mathbf{1}^{red}$ we have completed a three-membered electron-transfer series consisting of $\mathbf{1}^{ox}$, **1**, and $\mathbf{1}^{red}$. The broad electronic picture of this family reveals that the cobalt center remains divalent, and formally, only one ligand spans the full redox range: from the dianion L^{2-} to the radical $L^{\bullet-}$ to the most well-known state in the literature, neutral L^0. Both $\mathbf{1}^{ox}$ and $\mathbf{1}^{red}$ are formally ligand mixed-valent species and exhibit full delocalization of the ligand-based π^* electron(s) over the two ligands. Interestingly, the addition (or removal) of a single electron manifests itself in large structural changes in the first coordination sphere of cobalt to accommodate the additional electron (or hole) in the ligand π^* orbitals (Figure 14). Arguably, the most dramatic changes in electronic structure occur in the transition from neutral **1** to monoanionic $\mathbf{1}^{red}$, in which the metal undergoes a spin-transition from high-spin in **1** to low-spin Co(II) in $\mathbf{1}^{red}$ as θ decreases sharply from 80° to 27°. The closed-shell dianionic state of α-iminopyridines is quite rare, having only been structurally characterized in a few magnesium complexes. Indeed, the L^{2-} ligand in $\mathbf{1}^{red}$ is probably stabilized by delocalizing its π^* electrons into a nearby $L^{\bullet-}$ ligand via the metal d_{xz} and d_{yz} orbitals. Since delocalization would be maximal when θ approaches 0, the 27° observed in $\mathbf{1}^{red}$ likely reflects a fine balance between maximizing the delocalization of the ligand π^* electrons while minimizing the steric repulsion between the 5-pyridyl proton and the diisopropylphenyl group of opposing ligands.

The DFT calculations have shown a clear electronic picture of **3** as $[(L^{\bullet-})(L^0)Co^{II}I]$, which is supported by spectroscopic and crystallographic data. Despite the inconclusive results of the DFT studies of **2**, its electronic structure appears to approach a trivalent cobalt species $[(L^{\bullet-})_2Co^{III}Me]$, although the contribution of an electronic structure that is the direct analogue of **3** seems significant too. Notably, the reaction of MeI and $\mathbf{1}^{red}$ to give **2** is not a typical oxidation reaction because the metal center does not undergo a two-electron oxidation. Rather, it is the combination of one-electron oxidations of the metal and the ligand that effects the overall reduction of Me^+. This is yet another example of harnessing redox-active ligands to mediate organometallic elementary steps that are normally attributed to the metal center.[32−37]

Collectively, $\mathbf{1}^{ox}$, **2**, and **3** form another three-membered series in our system, namely penta-coordinate cobalt species $(L^n)(L^m)CoX$ with ligand oxidation states n and m. This series is ideal for probing the issue of metal versus ligand oxidation since the chemical environment around the metal is preserved with only the exception of the X ligand. As the σ-donor strength of X increases, one would expect ligand field splitting to increase and eventually stabilize low-spin Co(III) with two ligand π^* radicals relative to Co(II) with one ligand radical, as illustrated in Figure 15. A puzzling question is the switching of high-spin Co(II) in $\mathbf{1}^{ox}$ to low-spin Co(II) in **3**. Perhaps, another way to formulate this question is to ask why is the triplet spin group state favored for $\mathbf{1}^{ox}$, but a singlet ground state for **3**? It is tempting in light of comparing $\mathbf{1}^{ox}$ and **3** to speculate that the low-lying excited state in **3** may actually be a triplet spin system with an electronic structure identical to $\mathbf{1}^{ox}$, which would correspond to spin-crossover at the cobalt center, $S_{Co} = 1/2 \rightarrow S_{Co} = 3/2$. However, because of the limited data we have for this excited state, we cannot distinguish between spin-crossover at the metal or a thermally accessible state with an unpaired arrangement of metal and ligand-based spins.

Acknowledgment. The authors thank Jörg Bitter, Heike Schucht, Kerstin Neurieder, and Andreas Göbels for technical assistance. C.C.L. thanks the Alexander von Humboldt Foundation for funding.

Supporting Information Available: Additional spectroscopic data, including the ^{1}H NMR spectra of $\mathbf{1}^{red}$ and **2**, the H,H-COESY spectra of **2** and **3**, and the plot of $\Delta\delta$ versus T^{-1}. This material is available free of charge via the Internet at http://pubs.acs.org.

(32) Blackmore, K. J.; Sly, M. B.; Haneline, M. R.; Ziller, J. W.; Heyduk, A. F. *Inorg. Chem.* **2008**, *47*, 10522.
(33) Ketterer, N. A.; Fan, H.; Blackmore, K. J.; Yang, X.; Ziller, J. W.; Baik, M.-H.; Heyduk, A. F. *J. Am. Chem. Soc.* **2008**, *130*, 4364.
(34) Haneline, M. R.; Heyduk, A. F. *J. Am. Chem. Soc.* **2006**, *128*, 8410.
(35) Blackmore, K. J.; Ziller, J. W.; Heyduk, A. F. *Inorg. Chem.* **2005**, *44*, 5559.
(36) Ringenberg, M. R.; Kokatam, S. L.; Heiden, Z. M.; Rauchfuss, T. B. *J. Am. Chem. Soc.* **2008**, *130*, 788.
(37) Rolle, C. J., III; Hardcastle, K. I.; Soper, J. D. *Inorg. Chem.* **2008**, *47*, 1892.